Coriolis forces and Rocking To Precession (RTP) free Oscillations of the Obelisco Lateranense

Gerardo De Canio, Marialuisa Mongelli, Ivan Roselli
ENEA-Italian National Agency for New Technologies, Energy and Sustainable Economic Development, Via Anguillarese,301 S.M. di Galeria, Roma, Italy

Sergio Lagomarsino, Michela Rossi
Dipartimento di Ingegneria delle Costruzioni, dell'Ambiente e del Territorio
Università di Genova Via Montallegro, 1 16145 Genova, Italy

Keywords:Obelisk, Obelisco Lateranense, Coriolis, RTP - Rocking To Precession

ABSTRACT
Within the Performance Based Approach for assessing the seismic vulnerability of the Egyptian Obelisk in Piazza S. Giovanni in Laterano of Rome, Italy, the DDP-Displacement Data Processing of pull release and shaking table tests of a 1: 6 reduced scale mock-up of the obelisk has been performed, identifying three well defined RTP phases of its free oscillations governed by the Coriolis forces: Rocking, Transition and Precession. The phase R is a stable yet decaying rocking around the rotation axis (the base edges), in which the rotation is prevalent with respect to nutation and precession around the other axes. The phase T is an unstable transition, activated at a critic angular velocity, in which precession and nutation become more significant and comparable with the rocking rotation. The phase P is a table yet decaying precession, where the dynamic of the block is characterized by the prevalent precession around the vertical axis. During the phase R, the obelisk half rotates around the rocking axis, with constant decay of the maximum rotation angle after each impact. It is also notable, during phase R, the persistence level of the acceleration peak at each impact.

1 THE OBELISCO LATERANENSE

The Egyptian obelisk at Piazza S. Giovanni in Laterano is one of the greatest historic, artistic and archaeological monuments in Rome.



Figure 1. The Obelisco Lateranense in Roma.

It is 32 m high, its weight is 550 ton and was excavated as a single block from the Aswan quarries in Egypt at the age of the XVIII dynasty (15th century B.C.). It was transported, but not erected, to the Iper-Sout Sanctuary in Karnak by Thutmosis III (1504-1450 B.C.). The erection was done 17 years later by Thutmosis IV (1425-1417 B.C.), and it was positioned at the rear part of the Sanctuary aligned in axis with his father jubilee chapel and with the temple of Amenophis IV (Akhenoten). Then, the Obelisk remained in Karnak until the IVth century A.D. when the roman emperor Constantine the Great decided to move it to Constantinople. During the transportation, while the obelisk was at the Alexandria port waiting for being embarked, the emperor died and everything stopped. The resumption of the transportation happened 22 years later, when emperor Constantius II (337-371 A.D.) decided to change the destination and

to locate the obelisk at the Circus Maximus in Rome instead of Constantinople. The obelisk stood at the Circus Maximus until the VIth century (541-552 A.C.) when it fell down and broke in three pieces: this was the destiny of all the other Obelisks in Rome. It is not historically clear if this obelisk was broken by the Ostrogoths lead by Totila or by iconoclastic catholic fevers. Anyway, during the middle ages, the obelisk was disremembered and covered by sediments: until 1587 when pope Sisto V decided to rescue the obelisk and install it at the current location of Piazza San Giovanni in Laterano. The famous architect Domenico Fontana was committed for this complex operation: he rescued the obelisk and made the restoration connecting the three large fragments in which the obelisk was broken with innovative technological solutions, i.e. by means of "crux joints" elements connecting the blocks with each other (De Canio et al. 2011). To present day, the obelisk stands on a 10m tall pedestal and the total height of the monument is 45 m, including the cross on the top.

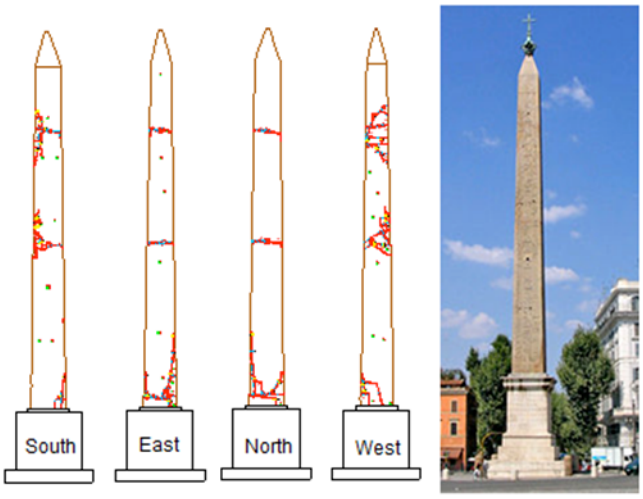


Figure 2. The three blocks of the Obelisco Lateranense.

2 ASSESSING THE OBELISK VULNERABILITY

The expected structural damages of this obelisk due to settlement, vibrations or earthquake are sliding or rocking of the blocks when the horizontal inertial forces are exceeding certain limits. An extensive in situ and laboratory experimental tests was carried out to identify the dynamic response of the obelisk by means of in situ monitoring and shaking table tests on a 1:6 reduced scale mock-up. The three blocks of granite are connected by two hinges with unknown binding degree, given that the rotational Degree of Freedom is blocked. The in situ investigations by Non Destructive Analyses (NDT) have highlighted the "crux joints" connecting the three blocks and the complex positioning of the blocks of granite at the base of the obelisk. The vulnerability evaluation and seismic reliability assessment was performed adopting the Performance Based Approach (PBA) on the basis of the damage measures detected by in situ NDT and during laboratory experimental tests, in order to define the proper limit states correlated to the damage measures and the reference seismic input (Lagomarsino et al. 2010). The adopted methodology is based on the DDP of the displacement field detected by the innovative 3DVision system at the ENEA Casaccia laboratories for direct measurement of the displacement of selected structural nodal points during shaking table experimental tests. The mechanical properties of the hinges were assessed by NDT and recursive optimization procedure of the kinematics of the three blocks and finite element numerical model (Mongelli et al. 2010) upgraded via Displacement Data Processing (DDP). Therefore, after the in situ structural monitoring and Non Destructive Investigations, the shaking table experimental campaign has been carried out to verify its performance on the basis of the dynamics behaviours of the structure during the experimental tests.

2.1 In situ investigation

The following in situ investigations has been carried on for the structural evaluation of the obelisk): a) structural monitoring and dynamic characterization by environmental vibrations; b) Non-Destructive Analyses for the mechanical characterization of materials and joint connections of blocks.

2.1.1 Vibrations by traffic

The main vibration forcing for the obelisk is due to the vehicle flux from via dell'Amba Aradam, regulated by a traffic light which has the red and green light duration of 50 sec and 80 sec. The N-S Auto Spectral Density spectrogram of the traffic induced vibrations is shown in Figure 3, duration = 1800 sec, with peaks at 1.3 Hz and 6.1 Hz corresponding to the N-S principal frequencies of the Obelisk in the elastic phase (De Canio et al. 2011). The frequency distribution of the traffic acceleration peaks is shown in Figure 4, where the N-S and E-W location of the accelerometers are also shown.

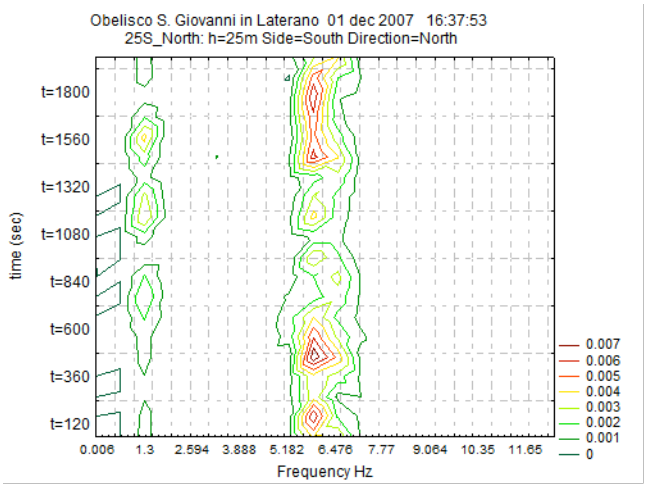


Figure 3. Auto Spectral spectrogram of traffic induced vibrations, duration: 1800 sec.

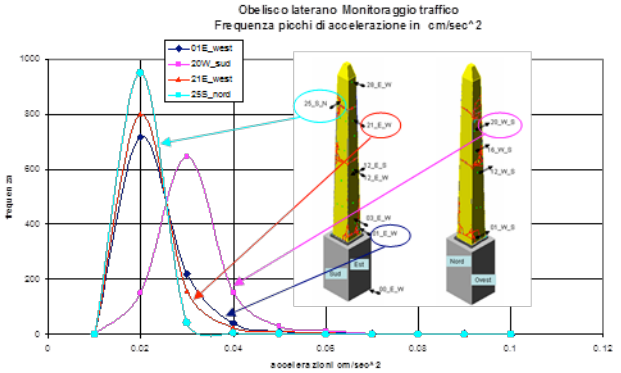


Figure 4. Frequency distribution of the acceleration peaks (cm/sec^2).

2.1.2 NDT investigations

Up to 4 zones have identified to characterize the geometrical and mechanical behaviours of the obelisk, therefore both sonic and radar investigations have been performed to identify the geometry and characterize the mechanical properties. The four zone are defined as follows: Zone type 1- base; Zone type 2 - sections with fractures repaired by Domenico Fontana using granite blocks from ancient roman monuments; Zone type 3- Joints between blocks; Zone type 4: Granite in good conditions (no fractures). Knowing the differences between the mechanical characteristics of the four representative zones is possible to make a parametric analysis of the dynamic response of the Obelisk with respect to the mechanical characteristics of the zone type 4 assuming different values of the mechanical properties of the granite within the minimum and maximum values in literature. For each value of the mechanical properties for the type 4 zone, the properties for the zone N° 1,2,3 have been assessed according the sonic and radar NDT experimental results. Table 1 and Figure 5 show the mechanic properties at different zones of the obelisk normalised to the properties of the integer granite zone.

Table 1. Normalised mechanic properties of the obelisk.

Zone	location	Parameter
1	Base 0 m	0.36
1	Base 1m	0.27
2	fractures	0.39
3	Joint 2-3	0.55
3	Joint 1-2	0.44
4	Granite	1. (Reference)

The sonic, ultrasonic and radar NDT results allowed to verify the presence of iron staffs and bronze plates at the base of the Obelisk and also the presence of the joints with crux to avoid sliding and rotation between the three blocks.

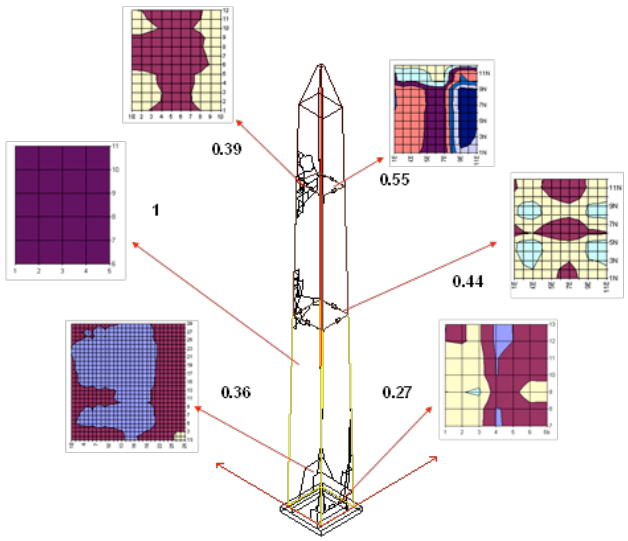


Figure 5. Normalised mechanical properties at different zones of the obelisk.

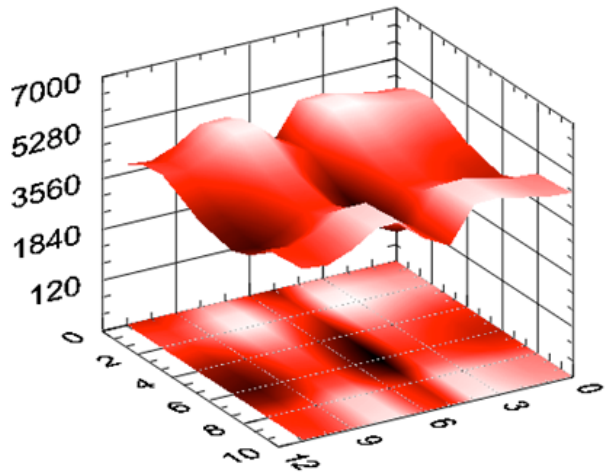


Figure 6. Mechanical properties at different zones of the obelisk normalised to the value of Zone 4 (integer granite).

3 NUMERICAL ANALYSIS AND SHAKING TABLE TESTS

A 1:6 reduced scale mock-up of the obelisk, with the same hinge connections between the three blocks have been realized. The overall dimensions of the obelisk are shown in table 2.

As the original obelisk, also the mock-up is not base symmetric (cfr. Figure 7) and the geometry of the hinges does not allow sliding and rotation of the blocks. During the free rocking motion, at each impact the non-symmetry of the base activates a precession motion in the direction of the vertical axis and, by the Coriolis acceleration effect, the activation of the nutation motion perpendicular to both rocking and precession axes. This Rocking To Precession (RTP) transition motion has been registered during the free Rocking phase of the obelisk mock-up during the experimental tests.

Table 2. Dimensions of the three blocks (m).

N°	High	West	North	East	South
1	14.13	2.83	2.80	2.84	2.91
2	9.41	2.29	2.58	2.31	2.56
3	8.72	1.94	2.30	1.91	2.29

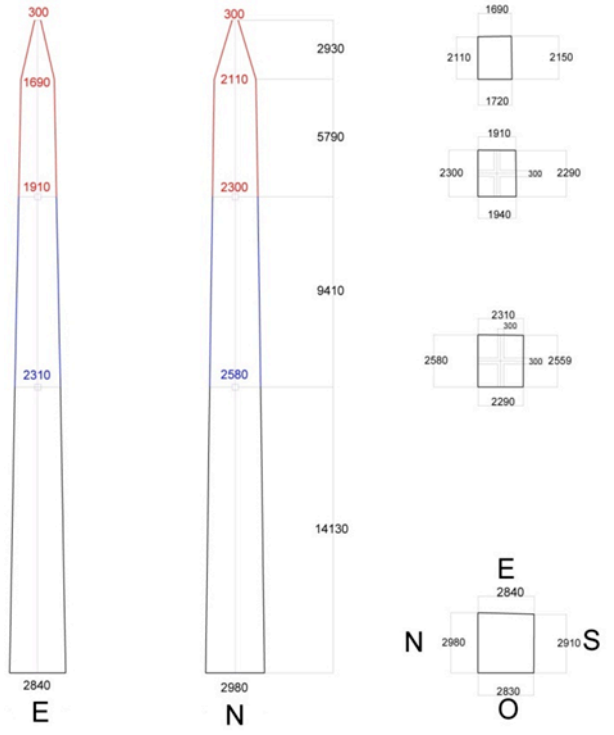


Figure 7.Dimensions of the Obelisco Lateranense.

The obelisk mock-up has been subjected to the following shaking table tests at the ENEA Casaccia laboratories of Roma, Italy: pull release, one directional and three directional earthquakes, one directional and three directional pulse. The tests have been performed on the single block, double blocks and three blocks configuration. The displacement data have been recorded by means of a new, innovative, high resolution 3-D optical movement detection and analysis tool named *3DVision*, tracking the dynamic displacement of special markers positioned at selected points of the structures during the shaking table tests, the light spots at the corners of each block in Figure 8 are the retro reflecting markers for 3DVision-DDP. The markers are located at selected Finite Element Model (FEM) nodes.



Figure 8. Positioning of the obelisk mock-up on the shaking table for pull release and seismic tests.

This monitoring technique allows measuring 3 axial absolute displacements with easy and fast test set-up, high accuracy and the possibility to link the 3D-motion time histories of the tracked markers with CAD drawings of the structure and validate the FE models in real time experimental data assimilation.

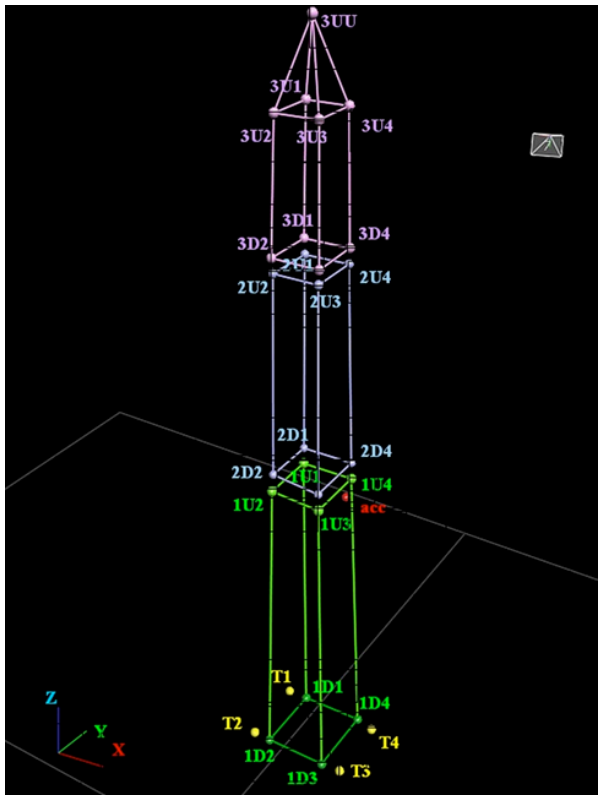


Figure 9. Marker connections and wireframe representation.

3.1 *Rocking of the obelisk as single block*

The dynamic response of the obelisk to earthquakes, as a free-standing block, is strongly non-linear and depends essentially on the critical angle α, the frequency parameter P and the spectral shape and intensity of the ground acceleration time history. In (De Canio et al. 2011) the rocking spectra and the dynamic response of the obelisk to earthquake, constant sine, Pulse A, B, C, D (Makris et al. 2011) has been performed through numerical integration of the (non-linear) equation of the rocking motion in presence of horizontal ground acceleration (Housner1963)

$$\ddot{\theta}(t) + p^2 \sin(sig(\theta)\cdot\alpha - \theta(t)) = \frac{\ddot{u}(t)}{g}\cos(sig(\theta)\cdot\alpha - \theta(t)) \qquad (1)$$

where u(t) and g are the horizontal and the gravity accelerations. The numerical model has been validated by 3DVision-DDP during the shaking table tests. The rocking pulse spectra and rocking seismic spectra obtained by numerical integration of eq. (1) are shown in the previous paper, together with the sine test numerical results. In Figure 10 are represented the rocking angle, the horizontal velocity and the acceleration time histories as results by the numerical integration of eq.(1).

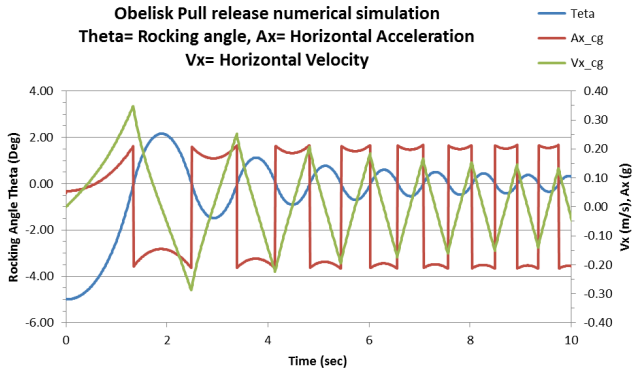


Figure 10. numerical integration of eq. 1: Pull release test.

This is a free rocking motion with initial conditions: θ(0) = -5° , Ax(0) = Vx(0) = 0. The graphs in Figure 10 show the velocity and acceleration singularities at each impact; it is also evident that, even if rocking angle, velocity and rocking period are decaying in time, the acceleration keep the same value at each impact. This is because the numerical model is mono-dimensional, geometrically linear and no variation of momentum is present due to external or internal forces.

3.2 *Pull release test on the 1:6 obelisk mock-up*

The same shape of Figure 10 happens to the real free rocking structure until *significant* variation of momentum is fed into the system due to external and/or internal forcing. This is what happened to the obelisk mock-up during the free rocking phase of the shaking table tests (cfr. Figure 11 and Figure 12), where the first rocking phase is stable, like a waked lagrangian top (Arnold, 1980), even with small geometric defects of the base geometry, i.e. the not symmetric base of obelisk mock-up.

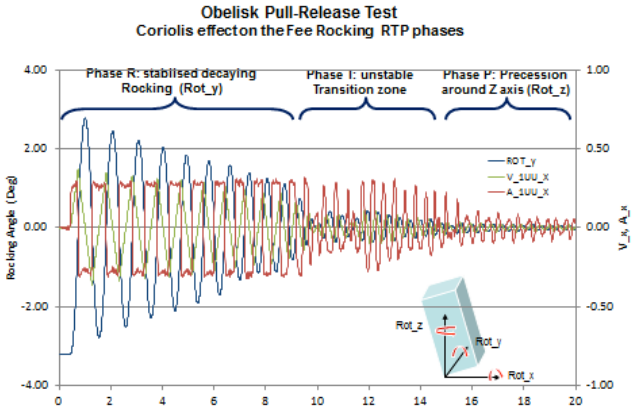


Figure 11.Pull-Release test: Rocking To Precession (RTP) motion of the obelisk.

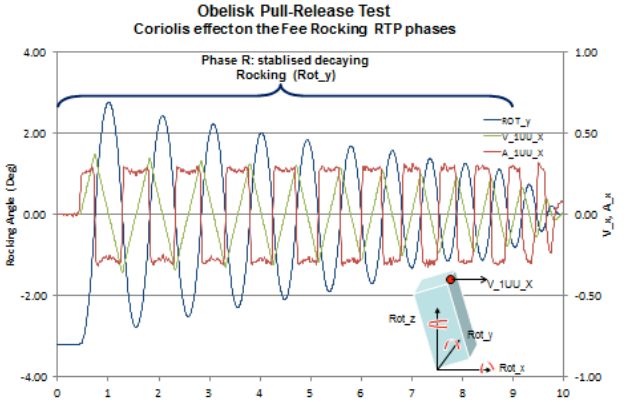


Figure 12.Pull-Release Test: Phase R (Stable Rocking) of the Obelisk. The markers displacement field have been analysed by 3DVision-DDP.

The 3DVision-DDP of the shaking table test results identified three well-defined phases in the free rocking of the obelisk, analogous to the transition from Rotation to Precession and Nutation for slow tops: **R** (Rocking), **T** (Transition), **P** (Precession).

- Phase **R**: Stable yet decaying rocking around Rotation axis (the base edge), in which the rotation is prevalent with respect to nutation and precession around the other axes;
- Phase **T**: Unstable Transition phase, activated at a critic angular velocity, in which

precession and nutation become more significant and comparable with the Rocking rotation;

- Phase **P**: Stable yet decaying Precession phase, where the dynamic of the block is characterized by the prevalent precession around the vertical axis.

It is notable, during phase R, the persistence level of the impact acceleration peaks. In this phase, after each rocking impact the obelisk small rotates around the nutation axis x (cfr. Figure 13 Rot_x) with persistent negative maximum peak values of the nutation angle.

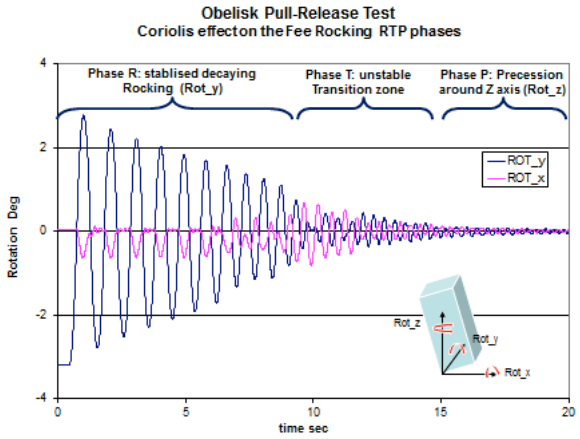


Figure 13. Transition from Rocking (Rot_y) to Nutation (Rot_x) due to Coriolis effect by not symmetric base.

The transition from the stable Rocking R to Precession P occurs because at each impact the precession angular velocity (along the vertical axis) increases by the infinitesimal change in the direction of the Rocking axis. This generates Coriolis acceleration forces feeding momentum along the so called nutation axis (cfr. Figure 15, Axis x^2), perpendicular to the plane defined by the rotation (Rocking) axis and the precession (vertical) axis. This happen *to any real free rocking system* until the rocking period (T=T(Ic,α,t,dθ/dt)) keeps a critic value. At this point, a quasi-chaotic transition phase with comparable precession, rotation and nutation starts. During this transition phase, the change of Rocking axis direction at each impact continues to feed small variation of momentum into the system, until rotation and nutation angular velocity become in-phase and the prevalent motion is a decaying precession. Note that the momentum variation happens when rotation axis changes direction at each impact, not when the angular velocity vector changes its versus. This is due to the directional (not positional) nature of the angular velocity vector.

3.3 3DVision-DDP in Generalized coordinates

The 3DVision-DDP at ENEA Casaccia Research Center analyses the trajectory of hundreds of markers positioned at selected nodal points of the structures under test. The trajectory of each marker is tracked by at least two infrared cameras (cfr. Figure14).

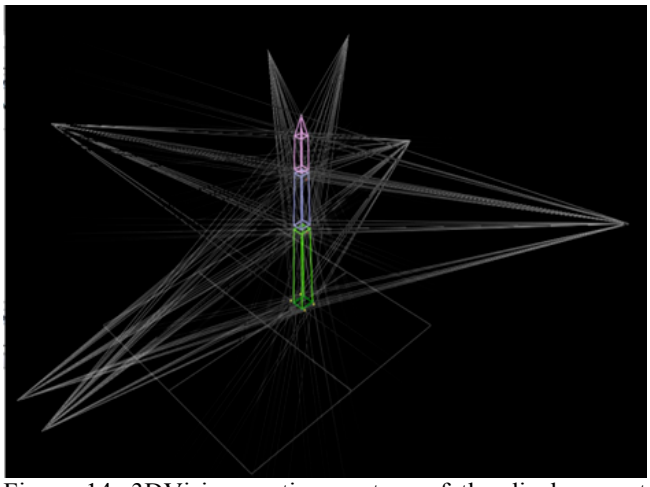


Figure 14. 3DVision motion capture of the displacement field during the ObeliscoLateranense shaking table tests.

Since all the trajectories are referred to a fixed reference point O_y (cfr. Figure 15), it is convenient to adopt the spherical coordinate system centred at O_y, then refer the equations of the motion to a moving generalized coordinate system (not necessarily orthogonal) connected to the obelisk by using a generalized coordinate transformation from spherical $S(\rho, \lambda, \varphi)$ to moving coordinate O_x ($x^1(t)$, $x^2(t)$, $x^3(t)$).

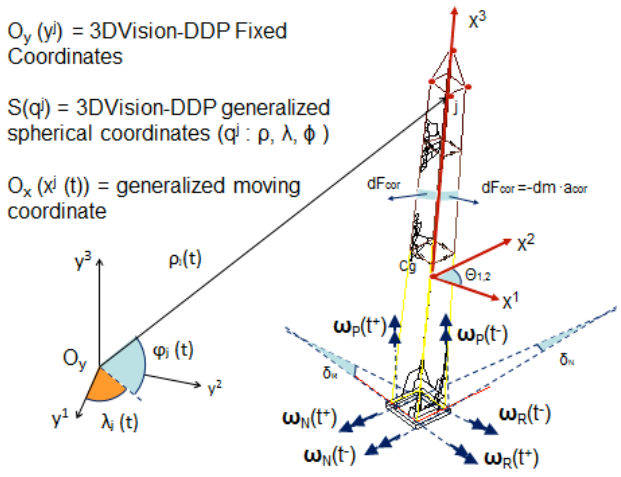


Figure 15. Coriolis forces and Rocking to precession (**RTP**) free rocking in Generalized coordinates.

The numerical integration of the governing equations, and all the physical quantities, are represented in the transformed space with time-dependent metric coefficients.

3.4 *Metric tensors and generalized coordinates transformation rules*

In this paragraph the tensor calculus properties, the transformation rules of invariance, covariance, contravariance and the generalized differential operators for the structural dynamic equations governing the motion of the obelisk in tensorial invariant form are summarized.

With reference to the Figure15, at each impact the rotation axis $\hat{r}$ twists by δ_R and the nutation axis $\hat{n}$ twists by δ_N. This generates a variation of the precession angular velocity ω_P by

$$d\vec{\omega}_P = (\vec{\omega}_R/|\omega_R|) \times \vec{\delta}_R + (\vec{\omega}_N/|\omega_N|) \times \vec{\delta}_N \quad (1)$$

which is associated to the Coriolis acceleration generating inertial Coriolis forces and momentum variation

$$\vec{a}_{cor} = 2 \cdot d\vec{\omega}_p \times \vec{v}_R;\ d\vec{F}_{cor} = -dm \cdot \vec{a}_{cor} \quad (2)$$

$$d\vec{M}_N = d\vec{F}_{cor} \times \vec{R}_{iN} = I_1(\vec{\omega}_R \times d\vec{\omega}_P)$$

$$d\vec{M}_N = I_1 d\vec{\omega}_N \quad (3)$$

$$d\vec{M}_R = d\vec{F}_{cor} \times \vec{R}_{iR} = I_3(\vec{\omega}_N \times d\vec{\omega}_P)$$

$$d\vec{M}_R = I_3 d\vec{\omega}_R \quad (4)$$

Equations 1, 3 and 4 relate the variation of rotation, nutation and precession angular velocities to the real geometries of the obelisk at each impact. Replacing the differential operators and the vector representation in the equations 1-4 with their generalized representations we obtain the invariant forms:

$$d\omega^j{}_P = \varepsilon^{ijk}\omega_{Ri} d\delta_{Rk} + \varepsilon^{ijk}\omega_{Ni} d\delta_{Nk} \quad (5)$$

$$a^j{}_{cor} = 2 \cdot \varepsilon^{ijk}\omega_{Pi} v_{Rk} \quad (6)$$

$$F^j{}_{cor} = -dm\, a^j{}_{cor} \quad (7)$$

$$dM^j{}_N = I^j{}_k\, d\omega^k{}_N \quad (8)$$

$$dM^j{}_R = I^j{}_k\, d\omega^k{}_R \quad (9)$$

where $I^j{}_k$ are the components of the inertia tensor and ε^{ijk} is the antisymmetric operator of the vector cross product: the i^{th} component of $\vec{\omega} \times \vec{r}$ is $\varepsilon^{ijk}\omega_j r_k$

$$\varepsilon^{ijk} = \frac{1}{\sqrt{g}} \quad if\ ijk = cyclic\ (2,3,1,..) \quad (10)$$

$$\varepsilon^{ijk} = -\frac{1}{\sqrt{g}} \quad if\ ijk = anticyclic\ (3,2,1,.) \quad (11)$$

the equations 5,..9 represent the contravariant components of the vectors in generalized coordinates, the lower indexed quantities are transformed by covariance, the upper indexed by contravariance and are related by the metric tensor. In fact, in the general coordinate transformation from $O_y(y^j)$ to $O_x(x^k)$ defined by $y^j = y^j(x^k)$, the elementary arc length (.i.e. the metric) is

$$dS^2 = dy^v dy^v = g_{ik} dx^i dx^k \quad (11)$$

g_{ik} is the metric tensor defined by

$$g_{ik} = (\partial y^v/\partial x^i)(\partial y^v/\partial x^k) = G^v_i G^v_k \quad (12)$$

In the 3DVision-DDP spherical polar coordinates ρ, λ, φ, the eq.(11) become:

$$dS^2 = d\rho^2 + \rho^2 cos^2\varphi d\lambda^2 + \rho^2 d\varphi^2 \quad (13)$$

The metric tensor and the Jacobian are:

$$g_{11} = \rho^2 cos^2\varphi;\ g_{22} = \rho^2;\ g_{33} = 1.;\ g_{ij} = 0 \quad i \neq j$$

$$J = \sqrt{g} = (Det(g_{ik}))^{1/2} = \rho^2 cos\varphi \quad (14)$$

The previous and all the other formula are obtained following the tensor calculus rules, the summation convention over repeated (dummies) and not repeated (free) indices is applied. Invariant quantities (scalars) not depending from the reference system don't have indices: $\phi(y^v) \equiv \phi(x^k)$.

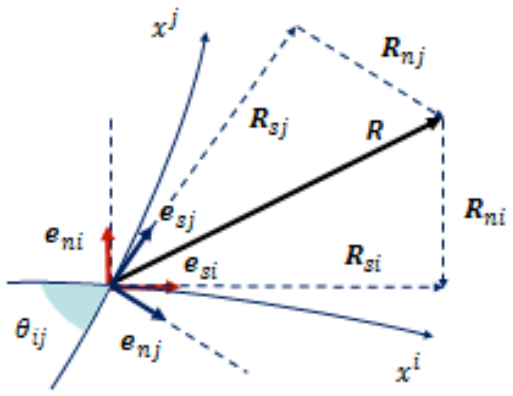


Figure 16. Physical components of a vector and its covariant and contravarant components.

The vector quantities are defined with their lower indexed covariant and upper indexed contravariant components

$$R_i = g_{ik}R^k;\ R^k = g^{jk}R_j \qquad (15)$$

which are related to the projection of the vector **R** on the tangent $\mathbf{R_{si}}$ and normal $\mathbf{R_{ni}}$ to the generalized coordinates by eq. (16) and (17).

The tangent and normal projection of the vector R on the generalized coordinate x^k are related to the covariant and contravariant components of the vector by

$$\boldsymbol{R}_{si} = \boldsymbol{e}_{si}R_i = (1/\sqrt{g_{ik}})\,R_k \qquad (16)$$

$$\boldsymbol{R}_{ni} = \boldsymbol{e}_{ni}\,R^i = (1/\sqrt{g^{ik}})\;R^k \qquad (17)$$

The angle θ_{ij} between the coordinate lines in Figure 16 is related to the metric coefficients by

$$\theta_{ij} = \sin^{-1}\left(\sqrt{g}/(\sqrt{g_{ii}g_{kk}}\right) \qquad (18)$$

3.5 Dynamics of the obelisk in generalized coordinates

The transformation $O_y(y^j) \rightarrow O_x(x^k)$ is governed by the coefficients ${G_k}^j$ defined in eq. (12) And the displacement, velocity and acceleration fields are

$$y^j = {y_{0x}}^j + {G_k}^j x^k \qquad (19)$$

$$\dot{y}^j = \dot{y}_{Ox}{}^j + {G_k}^j \dot{x}^k + \dot{G}_k{}^j x^k \qquad (20)$$

$$\ddot{y}^j = \ddot{y}_{ox}{}^j + \ddot{G}_k{}^j x^k + 2\dot{G}_k{}^j \dot{x}^k + \dot{G}_k{}^j \ddot{x}^k \qquad (21)$$

the first two terms in eq. (21) are the transport acceleration a^t, the third term is the Coriolis acceleration a^c and the fourth term is the relative acceleration a^r. The first and second time derivatives of the transformation coefficients are related to the angular velocity components by the skew symmetric tensor ε_{vik}

$$\dot{G}_k{}^j = \sum_{i=1}^{3} G_i{}^j \varepsilon_{vik}\omega^v \qquad (22)$$

therefore

$$\dot{y}^j = \dot{y}_{Ox}{}^j + {G_k}^j \dot{x}^k + \sum_{i=1}^{3} G_i{}^j \varepsilon_{vik}\omega^v \qquad (23)$$

$$\ddot{y}^j = \ddot{y}_{Ox}{}^j + {G_k}^j \ddot{x}^k + 2\sum_{i=1}^{3} G_i{}^j \varepsilon_{vik}\omega^v \dot{x}^k +$$

$$+{G_k}^j[(\omega_r x^r)\omega^q - (\omega_r \omega^r)x^q] +$$

$$+ \sum_{i=1}^{3} G_i{}^j \varepsilon_{vik}\dot{\omega}^v x^k \qquad (24)$$

Equations (19), (23) and (24) are the generalized representation of displacement, velocity and acceleration of the markers in the fixed frame of reference $O_y(y^j)$ expressed in generalized coordinates $O_x(x^k(t))$ which rotate and translate with respect to O_y. The correspondence between the vector representation and the generalized coordinates are reported in tables 3 and 4, see also (Borisenko et al. 1979) and (Wrede 1972).

Table3. vector operators in generalized coordinates

Vector	Components
$\vec{\boldsymbol{V}}_{\mathbf{Ox}}$	$\dot{y}_{cg}{}^j$
$\vec{\boldsymbol{V}}_{\mathbf{a}}$	${G_k}^j \dot{x}^k$
$\vec{\boldsymbol{\omega}} \times \vec{\boldsymbol{r}}$	$\sum_{i=1}^{3} G_i{}^j \varepsilon_{vik}\omega^v x^k$
$\vec{\boldsymbol{a}}_{\mathbf{Ox}}$	$\ddot{y}_{cg}{}^j$
$\vec{\boldsymbol{a}}_{\mathbf{a}}$	${G_k}^j \ddot{x}^k$
$2\vec{\boldsymbol{\omega}} \times \vec{\boldsymbol{V}}_{\mathbf{a}}$	$2\sum_{i=1}^{3} G_i{}^j \varepsilon_{vik}\omega^v \dot{x}^k$
$\vec{\boldsymbol{\omega}} \times (\vec{\boldsymbol{\omega}} \times \vec{\boldsymbol{r}})$	${G_k}^j[(\omega_r x^r)\omega^q - (\omega_r \omega^r)x^q$
$\vec{\boldsymbol{\omega}} \times \vec{\boldsymbol{r}}$	$\sum_{i=1}^{3} G_i{}^j \varepsilon_{vik}\dot{\omega}^v x^k$

Table4. description of the vector operators

Vector	description
$\vec{\boldsymbol{V}}_{\mathbf{Ox}}$	$O_x$traslation velocity
$\vec{\boldsymbol{V}}_{\mathbf{a}}$	Apparent velocity
$\vec{\boldsymbol{\omega}} \times \vec{\boldsymbol{r}}$	Apparent angular velocity
$\vec{\boldsymbol{a}}_{\mathbf{Ox}}$	O_xTraslation acceleration
$\vec{\boldsymbol{a}}_{\mathbf{a}}$	Apparent acceleration
$2\vec{\boldsymbol{\omega}} \times \vec{\boldsymbol{V}}_{\mathbf{a}}$	Coriolis acceleration
$\vec{\boldsymbol{\omega}} \times (\vec{\boldsymbol{\omega}} \times \vec{\boldsymbol{r}})$	Centripetal acceleration
$\vec{\boldsymbol{\omega}} \times \vec{\boldsymbol{r}}$	Apparent angular accel.

With reference to Figure 15, the coordinate transformations useful for 3DVision-DDP

$$O_y(y^j) \rightarrow S(q^j(x^k(t)) \rightarrow O_x(x^k(t)) \qquad (25)$$

are governed by the time-dependent metric coefficients. The general form (11) and (12) of the metric coefficients become

$$g_{ik}(t) = G_i^v(t)G_k^v(t) \qquad (26)$$

The rigid body motion of the moving generalized coordinates is described by the translation y_0 and the three rotations of the Euler angles θ,φ,ψ. The components of the angular velocities along the generalized axes x^k, in terms of covariant components (see Figure 17), are:

$$\omega_1 = \dot{\theta},\ \omega_2 = \dot{\varphi}sin\,\theta\,,\ \omega_3 = \dot{\psi} + \dot{\varphi}cos\theta \qquad (27)$$

which are transformed in the Cartesian ω_{yi} of the angular velocities in the reference $O_y(y^k)$ by the metric coefficients g_{ik}

$$\omega_{yi}=(1/\sqrt{g_{ik}}) \cdot \omega_k \quad (28)$$

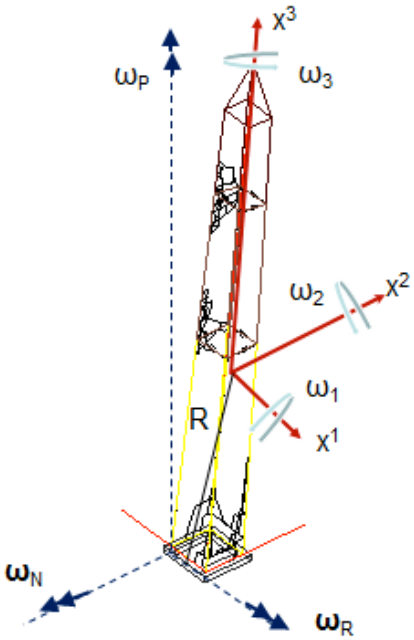


Figure 17. Physical components of the angular velocity and their covariant and contravariant components ω_k in the moving generalized coordinates x^k.

The balance between kinetic and potential energy during the motion, in terms of rocking angle, is governed by

$$E = 0.5 \cdot I_1^1(\theta)^2 + (M_3)^2/(2I_3^3) + mgRcos\theta + \\ +(M_P - M_3 cos\theta)^2/(2I_1^1 sin^2\theta) \quad (29)$$

and the condition for stable rocking (phase R) for the obelisk is related to the covariant component ω_3

$$\omega_3 < (4mgRI_1^1)^{1/2}/I_1^3 \quad (30)$$

which transforms by covariance with the cartesian components

$$\omega_{yk}= \omega_j/\sqrt{g_{i3}} \quad (31)$$

where $I_1^1=I_2^2>>I_3^3$; m is the mass of the obelisk; R is the distance of Cg by the rocking axis; ω_{yk} are the Cartesian components of the angular velocity. The stability condition for the rocking (phase R) in eq. (30) is the inverse of the stability condition for sleeping top described by (Arnold 1980).

4 CONCLUSIONS

The displacement data processing (DDP) during shaking table experimental tests allow the vulnerability evaluation and seismic reliability assessment on the basis of the damage measures directly in terms of relative displacements in the structures. The methodology is based on the 3DVision system at the ENEA Casaccia laboratories for direct measurement of the displacement of selected structural nodal points during shaking table tests. The displacement field is referred to a fixed reference and the vector operators describing the dynamics of the system under test are represented in generalized tensorial form. The 3DVision-DDP of the shaking table test on a 1:6 reduced model of the Obelisco Lateranense in Rome, Italy, identifies three well-defined phases in the free rocking of the obelisk: **R** (Rocking), **T** (Transition), **P** (Precession).

- Phase **R**: Stable yet decaying rocking around Rotation axis (the base edge), in which the rotation is prevalent with respect to nutation and precession around the other axes;
- Phase **T**: Unstable Transition phase, activated at a critic angular velocity, in which precession and nutation become more significant and comparable with the Rocking rotation;
- Phase **P**: Stable yet decaying Precession phase, where the dynamic of the block is characterized by the prevalent precession around the vertical axis.

The transition from the stable Rocking **R** to Precession **P** occurs because at each impact the precession angular velocity increases by the infinitesimal change in the direction of the Rocking axis. This generates Coriolis acceleration forces with momentum variation along the nutation axis, perpendicular to the plane defined by the rotation (Rocking) axis and the precession (vertical) axis. This happens *to any real free rocking system* until the rocking period (T=T(Ic,α,t,dθ/dt)) and the precession angular velocity keep critical values.

REFERENCES

Arnold, V.I., 1980. Mathematical Methods of Classical Mechanics. *Dover Publications, Inc. 1980,* New York, (NY).

Borisenko, A.I., Turapov, I.E., 1979. Vector and tensor analysis with applications. *Dover Publications, Inc. 1979,* New York, (NY).

De Canio, G., Baldini, M., Bonifazi, S., Colucci, A., Di Biagio, F., Fabrizi, G., Giaquinto, P., Mongelli, M, Tatì, A., 2011. Structural evaluation of the egyptian obelisk of San Giovanni in Laterano in Roma.*Proc. ART'11' 10th int. conf. on Non Destructive investigations and micro analysis for diagnostics of cultural and environmental heritage*, Florence, Italy.

De Canio, G., Clemente, P., Mongelli, M., Roselli, I.,Rinaldis, D., Saitta, F., Lagomarsino, S., Rossi, M. , 2012.Performance Based Assessment of the ObeliscoLateranense in Roma. *SAHC2012 October 15-17,* Wroclaw, Poland.

De Canio, G. ,1983.. Spazi di Rjeman e algebra tensoriale: applicazioni in fluidodinamica; Parte I[a] Fondamenti matematici; Parte II[a] Soluzioni numeriche e applicazioni. *Report No. ENEA FT-WHB/16 and 17 CSN 1983,* Roma, Italy.

Housner, G. W. , 1963. The Behavior of Inverted Pendulum Structures during Earthquakes. *Bulletin of the Seismological Society of America*. 53(2): 404-417.

Lagomarsino, S., Resemini, S., 2009. The Assessment of Damage Limitation State in the Seismic Analysis of Monumental Buildings.*EarthquakeSpectra*, 25: 2, pp. 323-346.

Lagomarsino, S., Modaressi, H., Pitilakis, K., Bosiljkov, V., Calderini, C., D'Ayala, D., Benouar, D., Cattari, S., 2010. PERPETUATE Project: the Proposal of a Performance-based Approach to Earthquake Protection of Cultural Heritage. *Advanced Material Research*, 133-134: 1119-1124.

Makris, N., Konstantinidis, D., 2011. The Rocking Spectrum and the Shortcomings of Design Guidelines. *Report No. PEER-01/07*, Berkeley, CA.

Mongelli, M., De Canio, G., Roselli, I., Colucci, A., Tatì, A., 2010. 3D motion capture and FEM analysis for shaking table tests at ENEA Casaccia Research Center. In: *Proc. 14 ECEE*2010, Ohrid, Macedonia.

Wrede, R.C., 1972. Introduction to vector and Tensor analysis. *Dover Publications, Inc. 1972,* New York, (NY)